INTERNATIONAL JOURNAL OF OPTIMIZATION IN CIVIL ENGINEERING
Int. J. Optim. Civil Eng., 2024; 14(4):553-572

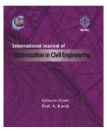

SEISMIC CONTROL OF MAGNETO-RHEOLOGICAL DAMPER-EQUIPPED STRUCTURES USING SLIDING SECTOR CONTROL

M. Nikpey[1], M. Khatibinia[1], and H. Eliasi [2*, †]
[1]*Department of Civil Engineering, University of Birjand, Birjand, Iran*
[2]*Department of Electrical Engineering, University of Birjand, Birjand, Iran*

[DOI: 10.22068/ijoce.2024.14.4.608]

ABSTRACT

In recent years, semi-active control has been introduced as a promising method for the seismic control of structures, potentially combining the benefits of both passive and active control systems. Magneto-rheological damper (MR) is one of the semi-active devices and its dynamic model is expressed by the Bouc-Wen model. The sliding sector control (SSC) strategy as a robust control approach is a class of variable structure (VS) systems for linear and nonlinear continuous-time systems with a special type of sliding sector using a new equivalent sector control. The purpose of this study is to evaluate the effectiveness of the SSC strategy in determining the optimal voltage of MR at each step of time. For a numerical example, a three-story benchmark shear structure is considered subjected to normal (100%), high (150%), and low (50%) excitation levels of the El Centro earthquake. The results of the numerical simulations show that the semi-active control system consisting of the SSC strategy and an MR damper can be beneficial in reducing the seismic responses of structures. Furthermore, the efficiency of the SSC strategy is also compared against that of the fuzzy and clipped-optimal controllers. Comparative results of the numerical simulation confirm the robustness and ability of the SSC strategy.

Keywords: Magneto-rheological Damper; Structural Control; Semi-active Control; Sliding Sector Control.

Received: 15 September 2024; Accepted: 2 November 2024

1. INTRODUCTION

Effective control of structures and reducing their seismic response under seismic excitations have attracted many researchers' concern in the field of civil engineering [1, 2]. Structural control is an emergent discipline that has witnessed significant acceptance and evolution

[*]Corresponding author: Department of Electrical Engineering, University of Birjand, Birjand, Iran
[†]E-mail address: h_eliasi@birjand.ac.ir (H. Eliasi)

over the past few decades. Structural control systems are generally categorized into four primary types: active, passive, semi-active, and hybrid control systems. The semi-active control system was first introduced in the early 1920s. In the structural engineering, the initial implementation of semi-active structural control for systems subjected to environmental loads was reported by Hrovat et al. [3]. The development and empirical evaluation of semi-active control systems for structural applications have gained considerable attention in the last few decades. These properties can be calibrated based on stimulus feedback or measured responses. In a semi-active control framework, the controller processes feedback measurements and generates appropriate signals for the semi-active devices. The control forces enhance the mechanical characteristics of the semi-active control system through judicious adjustments of the control algorithm [4]. Numerous studies have substantiated that well-executed semi-active control systems exhibit markedly superior performance compared to passive systems, demonstrating the capability to achieve functionalities typical of fully active systems [5].

In the context of employing magneto-rheological (MR) dampers, Dyke *et al*. [6] investigated the efficacy of a semi-active control strategy in a three-story structure. The results of this study indicated that the semi-active control system utilizing an MR damper outperforms a linear active controller in terms of mitigating the maximum displacement of the structure. Spencer *et al*. [7] concentrated their efforts on developing behavioral models for MR dampers and assessing their performance and proposed a novel model that rectified the limitations of prior models by accurately forecasting the response of MR damper under diverse operating conditions. Consequently, this model presented significant potential for the development of control algorithms and system evaluations. Jansen and Dyke [8] explored various semi-active control algorithms within a six-story structure utilizing MR dampers positioned on the first and second stories. Results revealed that every semi-active algorithm implemented enhanced the performance relative to the most effective passive controller available. Choi *et al*. [9] employed a semi-active fuzzy control strategy with a MR damper in a three-story shear structure under three intensity levels of the El Centro earthquake. Qin *et al*. [10] concentrated on the evaluation of the semi-active control system with MR dampers in reducing structural responses under earthquake and wind loads. Rodríguez *et al*. [11] formulated a force derivative feedback control algorithm for MR dampers and used this algorithm in an eight-story structure equipped with an elastomer-based isolation system. Results demonstrated that the algorithm substantially reduced the story displacements and accelerations and respectively yielded improvements of 55% and 76.5% in comparison with a passive isolation system. Khalid *et al*. [12] focused on modeling the dynamic behavior of MR dampers and devising their control strategies using neural networks. Mohebbi and Bagherkhani [13] conducted the optimal design of MR dampers on a ten-story shear structure using genetic algorithms. Kaveh *et al*. [14] developed a semi-active tuned mass damper (SATMD) to reduce vibrations in a 10-story building subjected to 4 different earthquake excitations. The SATMD consists of a mass damper connected in parallel with a MR damper. Cha and Agrawal [15] implemented the performance-based structural design utilizing MR dampers. Zabihi-Samani *et al*. [16] developed a wavelet-based fuzzy controller incorporating a cuckoo search, which minimized structural responses under near-earthquake excitations. Payandeh-Sani and Ahmadi-Nedushan [17] examined a multi-layer artificial neural network (ANN) for semi-active seismic response control with

[DOI: 10.22068/ijoce.2024.14.4.608]

MR dampers. Bathaei and Zahrai [18] employed a fuzzy logic algorithm to generate optimal damping forces in a semi-active control system based on a liquid MR damper. Moreover, Bagherkhani and Mohebbi [19] optimally designed MR dampers by considering design criteria and the effects of damper distribution along the structure's stories. Zizouni *et al*. [20] introduced a semi-active control strategy utilizing an electromagnetic damper with a sliding mode fuzzy hybrid controller, along with a cut-off optimization algorithm to determine the current required for the damper's operation. Jalali *et al*. [21] investigated the effect of soil-structure interaction on a five-story structure equipped with a semi-active MR damper under three different records. Payandeh-Sani and Ahmadi-Nedushan [22] investigated the semi-active control of structures with MR dampers using a fuzzy logic controller (FLC).

The sliding sector control (SSC) strategy introduced by Furuta [23] represents a subset of the state space with the quadratic stability. The strategy is based on a variable structure (VS) controller for both continuous and discrete time systems based on a sliding sector. The strategy shows the quadratic stability and eliminated the chattering phenomenon. The design of the SSC control was caused that the system state could move from the outside of the sliding sector to its inside in a finite time. Hence, this approach also prevent to apply an excessive control force to the system. Furthermore, the modifications of the SSC strategy were proposed in order to enhance its efficiency [23, 24].

To the authors' best knowledge, this study presents the first attempt to investigate the efficiency and capability of the SSC strategy in the semi-active control of structures equipped with an MR damper subjected to earthquake excitations. For achieving this purpose, the SSC strategy is first designed for a three-story building equipped with an MR damper under the normal (100%), high (150%) and low (50%) excitation levels of the El Centro earthquake. The performance of the SSC is evaluated through a comparative simulation with some other control techniques.

2. MATHEMATICAL MODEL OF STRUCTURE WITH A MR DAMPER

This section presents the mathematical model of an *N*-story shear frame building equipped with an MR damper located on the first story, as illustrated in Fig. 1. The MR damper is rigidly connected between the ground and the first floor of structure. The dynamic equation of the motion of the entire system is given as follows [13]:

$$\mathbf{M}\ddot{\mathbf{x}}(t)+\mathbf{C}\dot{\mathbf{x}}(t)+\mathbf{K}\mathbf{x}(t)=\boldsymbol{\Gamma}F(t)-\mathbf{M}\boldsymbol{\Lambda}\ddot{x}_g(t) \tag{1}$$

where **M**, **C**, and **K** represent the mass, damping, and stiffness matrices of the structure, respectively. The vector **x** indicates the vector of the relative displacements of the floors. $\ddot{x}_g(t)$ is the ground acceleration. $\boldsymbol{\Lambda}$ is the unit column vector. $\boldsymbol{\Gamma}$ is the position vector of the MR damper. *F* is the control force of the MR damper.

The mass, damping, and stiffness matrices of the shear frame are expressed in the following form:

[DOI: 10.22068/ijoce.2024.14.4.608]

$$\mathbf{M}=\begin{bmatrix} m_1 & 0 & 0 & \cdots & 0 \\ 0 & m_2 & 0 & \cdots & 0 \\ \vdots & \vdots & \vdots & \vdots & \vdots \\ 0 & 0 & 0 & \cdots & m_N \end{bmatrix} \tag{2}$$

$$\mathbf{K}=\begin{bmatrix} k_1+k_2 & -k_2 & & & 0 \\ -k_2 & k_2+k_3 & -k_3 & & \\ & & \ddots & & \\ & sym & & -k_{N-1} & k_{N-1}+k_N & -k_N \\ & & & & -k_N & k_N \end{bmatrix} \tag{3}$$

$$\mathbf{C}=\begin{bmatrix} c_1+k_2 & -c_2 & & & 0 \\ -c_2 & c_2+c_3 & -c_3 & & \\ & & \ddots & & \\ & sym & & -c_{N-1} & c_{N-1}+c_N & -c_N \\ & & & & -c_N & c_N \end{bmatrix} \tag{4}$$

where $m_i, k_i,$ and c_i are the mass, stiffness and damping of *i*the floor.

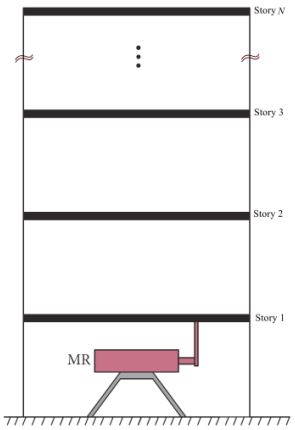

Figure. 1 An *N*-story shear frame building equipped with an MR damper

The vectors $\mathbf{\Lambda}$ and $\mathbf{\Gamma}$ are also defined as:

$$\mathbf{\Gamma}=\begin{bmatrix}-1 & 0 & 0 & \cdots & 0\end{bmatrix}^T \;;\; \mathbf{\Lambda}=\begin{bmatrix}1 & 1 & 1 & \cdots & 1\end{bmatrix}^T \tag{5}$$

Eq. (1) can be expressed in state-space form as follows [13]:

[DOI: 10.22068/ijoce.2024.14.4.608]

$$\dot{\mathbf{z}}(t) = \mathbf{A}\mathbf{z}(t) + \mathbf{B}F(t) + \mathbf{E}\ddot{x}_g(t) \tag{6}$$

$$\mathbf{y}(t) = \bar{\mathbf{C}}\mathbf{z}(t) + \bar{\mathbf{D}}F(t) + \mathbf{v} \tag{7}$$

where **z** is the state vector, **y** is the vector of measured outputs, and **v** is the vector of measured noise. The matrices **A**, **B**, **E**, $\bar{\mathbf{C}}$, and $\bar{\mathbf{D}}$ are defined as:

$$\mathbf{A} = \begin{bmatrix} \mathbf{0}_{N\times N} & \mathbf{I}_{N\times N} \\ -\mathbf{M}^{-1}\mathbf{K} & -\mathbf{M}^{-1}\mathbf{C} \end{bmatrix} \; ; \; \mathbf{B} = \begin{bmatrix} \mathbf{0}_{N\times 1} \\ \mathbf{M}^{-1}\boldsymbol{\Gamma}_{N\times 1} \end{bmatrix} \; ; \; \mathbf{E} = \begin{bmatrix} \mathbf{0}_{N\times 1} \\ \boldsymbol{\Lambda}_{N\times 1} \end{bmatrix} \tag{8}$$

$$\bar{\mathbf{C}} = \begin{bmatrix} -\mathbf{M}^{-1}\mathbf{K} & \mathbf{M}^{-1}\mathbf{C} \\ -\boldsymbol{\Gamma}_{1\times N}^{-1} & \mathbf{0}_{1\times N} \\ \mathbf{0}_{1\times N} & -\boldsymbol{\Gamma}_{1\times N}^{-1} \end{bmatrix} \; ; \; \bar{\mathbf{D}} = \begin{bmatrix} \mathbf{M}^{-1}\boldsymbol{\Gamma} \\ \mathbf{0}_{1\times N} \\ \mathbf{0}_{1\times N} \end{bmatrix} \tag{9}$$

3. MR DAMPER MODEL

Different mechanical models, including the Bingham model, Gamota and Filisko model, Bouc-Wen model, and modified Bouc-Wen model have been proposed to predict the modeling response of MR dampers [27]. The modified Bouc-Wen model can be used to accurately model the nonlinear behavior of MR damper (shown in Fig. 2) under complex and unpredictable conditions.

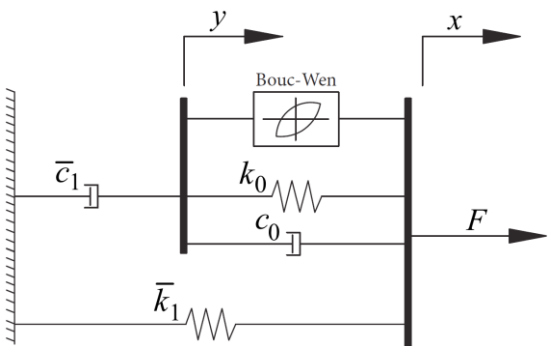

Figure. 2 Modified mechanical model of Bouc-Wen [24]

The MR damper force F, as, is calculated as follows:

$$F(t) = \bar{c}_1\dot{y} + \bar{k}_1(x - x_0) \tag{10}$$

The total force generated by the system can also be expressed as:

$$F(t) = \alpha\bar{z} + \mathrm{c}_0(\dot{x} - \dot{y}) + k_0(x - y) + \bar{k}_1(x - x_0) \tag{11}$$

[DOI: 10.22068/ijoce.2024.14.4.608]

The variable $\bar{z}$ is obtained using the following equation:

$$\dot{\bar{z}} = -\gamma|\dot{x}-\dot{y}|\bar{z}|\bar{z}|^{n-1} - \beta(\dot{x}-\dot{y})|\bar{z}|^{n} + A^{*}(\dot{x}-\dot{y}) \tag{12}$$

$$\dot{y} = \frac{1}{(c_0 + \bar{c}_1)}\left[\alpha\bar{z} + c_0\dot{x} + k_0(x-y)\right] \tag{13}$$

The parameters $A^{*}, \gamma, \beta,$ and n define the hysteresis loop's shape and scale, allowing adaptation to a specific damper's characteristics. In this model, $\bar{k}_1$ denotes the accumulator stiffness, and c_0 is viscous damping at high velocities. $\bar{c}_1$ is incorporated to account for the roll-off noted in the experimental data at low velocities, whereas k_0 manages stiffness at high velocities, and x_0 represents the initial displacement of spring $\bar{k}_1$ linked to the nominal damper force from the accumulator [27].

The current dependency of the damper force is implemented through a linear relationship of certain parameters with the applied voltage:

$$\begin{aligned} \alpha &= \alpha_0 + \alpha_b u_d \\ \bar{c}_1 &= \bar{c}_{1a} + \bar{c}_{1b} u_d \\ c_0 &= c_{0a} + c_{0b} u_d \end{aligned} \tag{14}$$

The variables denoted with an '*a*' subscript are determined at 0 V, while u_d represents a phenomenological factor that captures the system's dynamics through a first-order equation:

$$\dot{u}_d = -\eta(u_d - V) \tag{15}$$

4. SLIDING SECTOR CONTROL

Sliding Mode Control (SMC) is a nonlinear control method in which the controller input switches between two different states. This method allows the system states to reach a level known as the sliding surface in state space, where they then move in a sliding manner. This approach offers advantages, such as precision, robustness, easy tuning, and simple implementation. In the SMC method, as illustrated in Fig. 3 (a), a sliding surface is established for the system. Consequently, if the velocity and displacement of the structure do not remain on this sliding surface, a control force is applied according to the sliding mode control law to bring them back onto the sliding surface. By applying this control force, the velocity and displacement of the structure traverse the sliding surface. Therefore, an opposing control force must be exerted to keep the velocity and displacement of the structure on the sliding surface. This process continues until the system approaches a stable

[DOI: 10.22068/ijoce.2024.14.4.608]

point with zero velocity and displacement. However, in the SSC method, a sliding sector is established as depicted in Fig. 3(b). The advantage of defining a sliding sector is that when a control force is applied, causing the speed and displacement of the structure to fall within this sector, the same control system continues to operate without needing to apply a reverse force until the structure exits the sliding sector. The phenomenon of chattering is recognized as a limiting factor of the sliding mode method due to frequent switching or delays in switching. Consequently, excessive reversal of the control force at short time intervals may not be practically feasible and can lead to resonance in the system because of the limited switching frequency and delays in the controller. Therefore, the design of the SSC controller ensures that the system transitions from outside the sliding sector to within it in a constrained time frame [24].

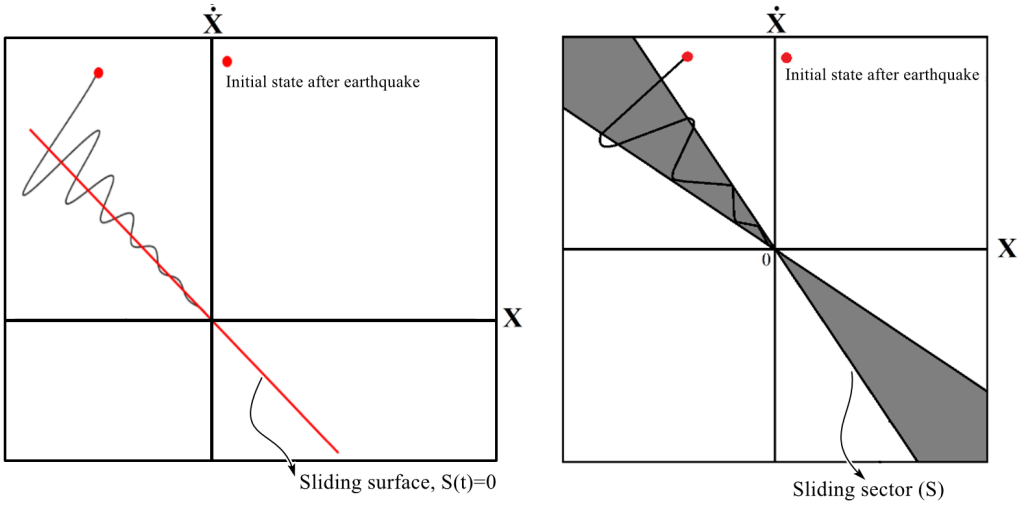

Figure 3. (a) Sliding surface, (b) sliding sector for a SDOF system [28]

4.1 PR–sliding sector

The Lyapunov function for a semi-active system is defined as follows [24]:

$$\mathrm{L}(\boldsymbol{z}) = \|\boldsymbol{z}\|_P^2 = \boldsymbol{z}^{\mathrm{T}}\mathbf{P}\boldsymbol{z} > 0 \;\; ; \;\; \forall \boldsymbol{z} \in \mathbb{R}^N \;\; , \;\; \boldsymbol{z} \neq 0 \tag{16}$$

For a structure with an MR damper, *P*–norm is expressed as follows:

$$\|\boldsymbol{z}\|_P = \sqrt{\boldsymbol{z}^{\mathrm{T}}\mathbf{P}\boldsymbol{z}} \;\; ; \;\; \boldsymbol{z} \in \mathbb{R}^N \tag{17}$$

where The matrix **P** is a symmetric positive-definite matrix.

A symmetric positive-definite matrix and semi-definite matrix **R** are defined for a second-order stable system that satisfies the following formula:

$$\dot{\mathrm{L}}(\boldsymbol{z}) = \boldsymbol{z}^{\mathrm{T}}(\mathbf{A}^{\mathrm{T}}\mathbf{P} + \mathbf{P}\mathbf{A})\boldsymbol{z} \leq -\boldsymbol{z}^{\mathrm{T}}\mathbf{R}\boldsymbol{z} \tag{18}$$

[DOI: 10.22068/ijoce.2024.14.4.608]

Consequently, the state space is partitioned into two distinct regions, wherein the aforementioned inequality holds true for a subset of elements and false for the remainder. To address a specific subset of the state space in inequality (18), the *PR*–sliding sector is established using the following formula. Within this sector, no control force is required, and the subsequent equation is defined using matrices **P** and **R**.

$$\mathrm{S} = \left\{ \boldsymbol{z} \middle| \boldsymbol{z}^{\mathbf{T}}(\mathbf{A}^{\mathbf{T}}\mathbf{P} + \mathbf{P}\mathbf{A})\boldsymbol{z} \le -\boldsymbol{z}^{\mathbf{T}}\mathbf{R}\boldsymbol{z}, \boldsymbol{z} \in \mathbb{R}^{N} \right\} \tag{19}$$

The simple form of sector mentioned in the above equation is as follows:

$$\mathrm{S} = \left\{ \boldsymbol{z} \middle| |\mathrm{s}(\boldsymbol{z})| \le \delta(\boldsymbol{z}), \boldsymbol{z} \in \mathbb{R}^{N} \right\} \tag{20}$$

where the linear function used to define the sliding surface is determined as follows:

$$\mathrm{s}(\boldsymbol{z}) = \mathbf{H}\boldsymbol{z}(t) \;\; ; \;\; \mathbf{H} \in R^{N} \tag{21}$$

and the quadratic function $\delta(\boldsymbol{z})$ is expressed as follows:

$$\delta(\boldsymbol{z}) = \sqrt{\boldsymbol{z}^{T}(t)\Delta\boldsymbol{z}(t)} \quad ; \quad \Delta = \mathbf{Q} - \mathbf{R} = r\mathbf{Q} \tag{22}$$

where r is a constant coefficient ranging from zero to one.

The matrix **P** is the solution to the Riccati equation referenced in Eq. (23), and **Q** is a symmetric positive semi-definite matrix.

$$\mathbf{A}^{T}\mathbf{P} + \mathbf{P}\mathbf{A} - \mathbf{P}\mathbf{B}\mathbf{B}^{T}\mathbf{P} + \mathbf{Q} = 0 \tag{23}$$

The derivative of the Lyapunov function defined in the *PR*–sliding sector satisfies the following inequality:

$$\dot{\mathrm{L}}(\boldsymbol{z}) = \frac{d}{dt}(\boldsymbol{z}^{T}\mathbf{P}\boldsymbol{z}) = \mathrm{s}^{2}(\boldsymbol{z}) - \delta^{2}(\boldsymbol{z}) - \boldsymbol{z}^{T}\mathbf{R}\boldsymbol{z} \le -\boldsymbol{z}^{T}\mathbf{R}\boldsymbol{z} \quad ; \; \forall \boldsymbol{z} \in \mathrm{S} \tag{24}$$

4.2 Design of SSC for the semi-active control of structures

For the semi-active control of structures, the design of the SSC technique is constructed based on moving the system state from the outside of the *PR*–sliding sector to its inside with VS control law, and then inside it the control input is considered equal to zero for ensuring the reduction of the *P*–norm. Thus, the SSC input is only considered as active state when the location of the system state is outside of the *PR*–sliding sector. To eliminate chattering phenomena on the boundary of the *PR*–sliding sector, the subsets of the *PR*–sliding sector including an inner sector $\mathrm{S_i}$ and an outer sector $\mathrm{S_o}$ are defined as [24]:

[DOI: 10.22068/ijoce.2024.14.4.608]

$$S_i = \left\{ \boldsymbol{z} \middle| |s(\boldsymbol{z})| \le \bar{\alpha}\delta(\boldsymbol{z}),\ \boldsymbol{z} \in R^N \right\} \tag{25}$$

$$S_o = \left\{ \boldsymbol{z} \middle| \bar{\alpha}\delta(\boldsymbol{z}) < |s(\boldsymbol{z})| \le \delta(\boldsymbol{z}),\ \boldsymbol{z} \in R^N \right\} \tag{26}$$

where the coefficient $\bar{\alpha}$ is a positive constant within the range of zero to one.

The control law for the system defined in Eq. (1) is defined as follows:

$$u(t) = \sigma(s(\boldsymbol{z}), \delta(\boldsymbol{z}))u_o(t) + (1 - \sigma(s(\boldsymbol{z}), \delta(\boldsymbol{z})))u_i(t) \tag{27}$$

$$\sigma(s(\boldsymbol{z}), \delta(\boldsymbol{z})) = \begin{cases} 0 & \boldsymbol{z} \in S_i \\ \text{unchanged} & \boldsymbol{z} \in S_o \\ 1 & \boldsymbol{z} \notin S \end{cases} \tag{28}$$

where $u_o(t)$ and $u_i(t)$ are expressed as:

$$u_i(t) = -\hat{g}^{-1}\bar{k}_1(\boldsymbol{z})\text{sgn}(s(\boldsymbol{z})) \tag{29}$$

$$u_o(t) = -\hat{g}^{-1}((\mathbf{HB})^{-1}\mathbf{HA}\boldsymbol{z}(t) + ((\mathbf{HB})^{-1}\bar{K}\bar{\beta}|s(\boldsymbol{z})| + \bar{k}_2(\boldsymbol{z}))\text{sgn}(s(\boldsymbol{z}))) \tag{30}$$

where $\bar{K}$ represents a positive constant. $\bar{k}_1(\boldsymbol{z})$ and $\bar{k}_2(\boldsymbol{z})$ are positive scalar functions. These variables, $\bar{K}$, $\bar{k}_1(\boldsymbol{z})$ and $\bar{k}_2(\boldsymbol{z})$, are subject to specific inequalities as follows:

$$\bar{K} > \max\left\{ \frac{\mathbf{HB}}{2}, \bar{K}_0 \right\} \tag{31}$$

$$\bar{k}_1(\boldsymbol{z}) > 0\ ;\ \bar{k}_2(\boldsymbol{z}) > (\mathbf{HB})^{-1}\max\left\{ \bar{\beta} - 1, 1 - \bar{\beta}^{-1} \right\} |\mathbf{HA}\boldsymbol{z}| \tag{32}$$

Furthermore, the choice of parameters $\hat{g}$ and $\bar{\beta}$ is dictated by the bounds of the uncertain parameter $\hat{g}$ as:

$$\hat{g} = \sqrt{\hat{g}_{\min}\hat{g}_{\max}}\ \ ;\ \ \bar{\beta} = \sqrt{\frac{\hat{g}_{\max}}{\hat{g}_{\min}}} \tag{33}$$

Addition, $\bar{K}_0$ signifies a positive constant that satisfies the conditions of a quadratic inequality:

$$2\bar{K}_0\alpha^2\bar{r}\mathbf{Q} + \mathbf{H}^T\mathbf{HA} + \mathbf{A}^T\mathbf{H}^T\mathbf{H} > 0 \tag{34}$$

[DOI: 10.22068/ijoce.2024.14.4.608]

5. DEVELOPMENT OF SEMI-ACTIVE CONTROLLER

The damping force generated by the MR damper is applied to the base-isolated structure under earthquake excitations. The damping force is produced by the electric voltage entering the MR damper. Further, the force of the MR damper can't be directly controlled by means of a controller. In this study, the clipped-optimal technique proposed by Dyke *et al*. [29] is used to convert the required control force into the equivalent voltage. The technique consists of an optimal controller that computes a desirable control force, F_c, and a clipping algorithm used to convert F_c into a control voltage, V. The SSC strategy is adopted as the optimal controller. The block diagram of the semi-active system is illustrated in Fig 4.

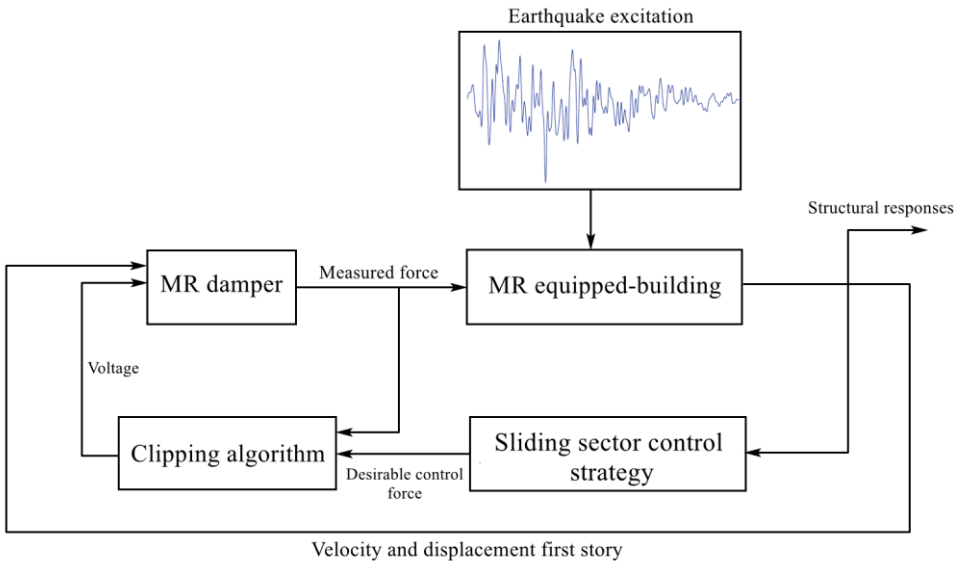

Figure 4. Block diagram of semi-active control system

The clipped-optimal technique is represented as follows [29]:

$$V = V_{\max} H\{(F_c - F_{\mathrm{MR}})F_{\mathrm{MR}}\} \tag{35}$$

where $H\{\bullet\}$ is the Heaviside function. $V_{\max}$ is the maximum input voltage of the MR damper. F_c is the optimal control force,

The algorithm is based on the difference between the desirable force and the measured force. If the amplitude of the measured force is lower than that of the control force and both forces are of the same sign, then the maximum voltage will be applied. Conversely, if F_c is smaller than F_{MR}, 0 V will be applied. This can be summarized as [29]:

[DOI: 10.22068/ijoce.2024.14.4.608]

$$V = \begin{cases} 0 & \text{if } |F_c| < |F_{\text{MR}}| \\ V_{\max} & \text{if } |F_c| < |F_{\text{MR}}| \cap F_c \times F_{\text{MR}} \geq 0 \end{cases} \quad (36)$$

6. NUMERICAL ANALYSIS

In this section, a numerical example is presented to investigate and assess the effectiveness of the SSC strategy for the seismic control of the MR damper equipped-structure under earthquake excitations. In this study, a three-story shear frame building as benchmark structure was used which was previously introduced in the studies by Dyke *et al*. [6] and was tested in the Structural Dynamics Laboratory at Notre Dame University. Table 1 displays the structural characteristics of the shear frame.

Table 1: Dynamic specification of the three-story shear frame

Story	Mass (kg)	Stiffness (kN/m)	Damping (N.s/m)
1	98.3	516	125
2	98.3	684	50
3	98.3	684	50

Furthermore, an MR damper with a maximum voltage of 2.25 V and a peak capacity of 3000 kN was employed. Its dynamic characteristics were listed in Table 2.

Table 2: Parameters of the modified Bouc-Wen model for the MR damper

Parameter	Value	Parameter	Value
c_{0a}	2100 N.s/m	α_a	14000 N/m
c_{0b}	350 N.s/mV	α_b	69500 N/mV
k_0	4690 N/m	γ	363×10^4 /m^2
$\overline{c}_{1a}$	28300 N.s/m	β	363×10^4 /m^2
$\overline{c}_{1b}$	295 N.s/mV	A	1107.2
$\overline{k}_1$	500 N/m	n	2
x_0	0	η	190/s

The model of the structure is subjected to the NS component of the 1940 El Centro earthquake (PGA=0.348g) shown in Fig. 5. Because the system in the experimental study was a scaled model, the earthquake was reproduced at five times the recorded rate [6].

6.1 Designing semi-active control system

As expressed in sections (4), the design of the SSC strategy for the structural seismic control depends on the specific parameters. These parameter values can be determined

[DOI: 10.22068/ijoce.2024.14.4.608]

through either an optimization process or the trial-and-error procedure. For this investigation, a trial-and-error procedure was utilized to identify parameter values that the seismic performance of the structure equipped with the MR damper was improved. The values of the parameters are equal to $r = 0.15, \alpha = 0.99, k_1(\boldsymbol{z}) = 752$ and $k_2(\boldsymbol{z}) = 613$.

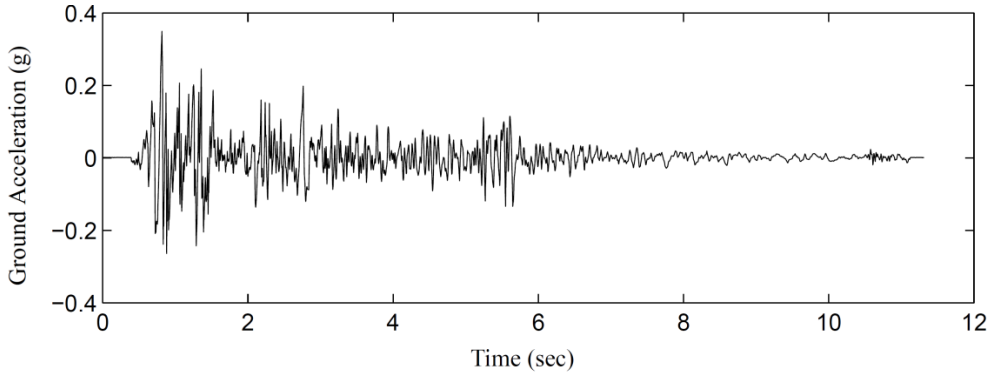

Figure 5. Time scaled NS component of the ground acceleration for the 1940 El Centro earthquake [4]

The studies implemented by Eliasi *et al*. [30] and Khatibinia *et al*. [31] showed that the elements of matrix **Q** were defined using coefficients derived from the values of stiffness and damping stories of the building. These coefficients can be determined through either an optimization problem or trial-and-error procedure. In this study, a trial-and-error procedure was employed to determine the components of matrix **Q**.

6.3 Assessment of the semi-active control strategy

To assess the reduction of the structural responses through the MR damper and SSC strategy, the seismic control of the structure was investigated under the normal (100%), high (150%) and low (50%) excitation levels of the El Centro earthquake. Two scenarios were also considered including: passive-on (constant 2.25 volts) and passive-off (constant zero volts), in order evaluate the effectiveness of the SSC strategy. The uncontrolled, passive-on, passive-off, and controlled (with SSC strategy) conditions were respectively presented by Unctrl'd, P-On, P-Off, and Ctrl'd. Figs. 6 to 8 show the time history of the drift and acceleration of the third floor in the Ctrl'd and Unctrl'd conditions. Results indicated that the semi-active control strategy considerably reduced the seismic responses of the third floor.

[DOI: 10.22068/ijoce.2024.14.4.608]

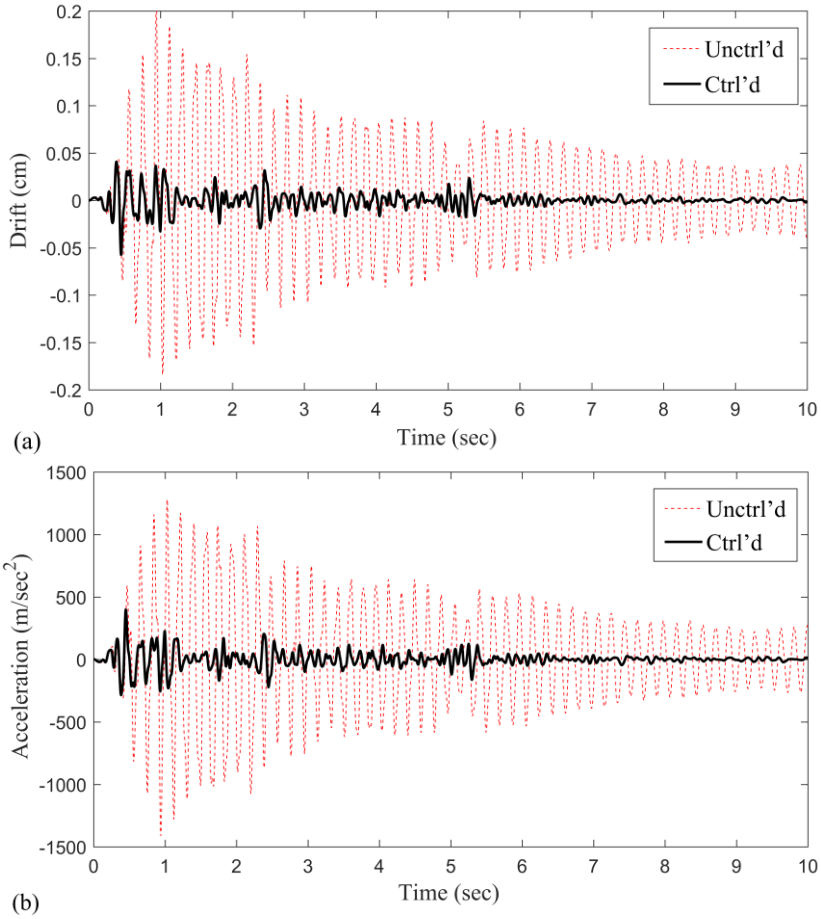

Figure 6. Time histories of responses on the third floor under the normal (100%) El Centro earthquake: (a) drift; and (b) acceleration

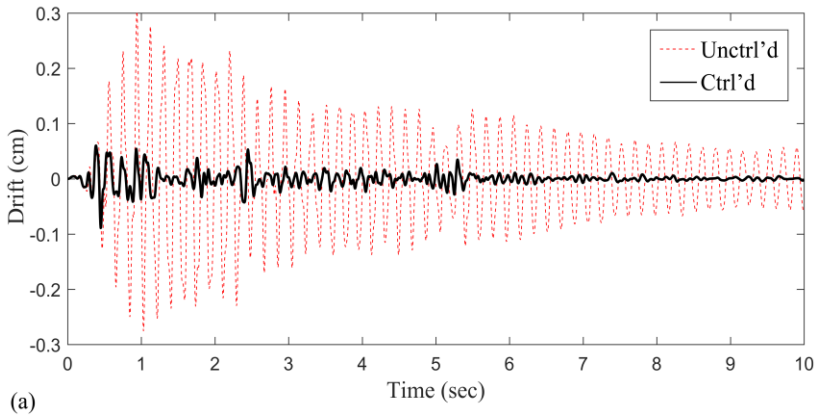

[DOI: 10.22068/ijoce.2024.14.4.608]

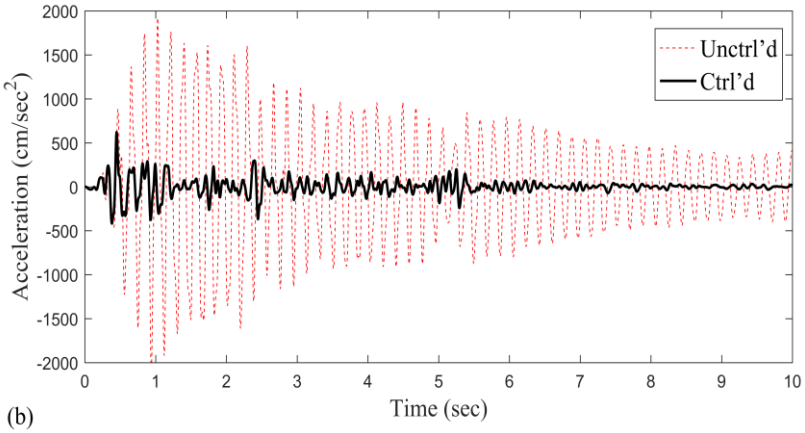

Figure 7. Time histories of responses in the third floor under the high (105%) El Centro earthquake: (a) drift; and (b) acceleration

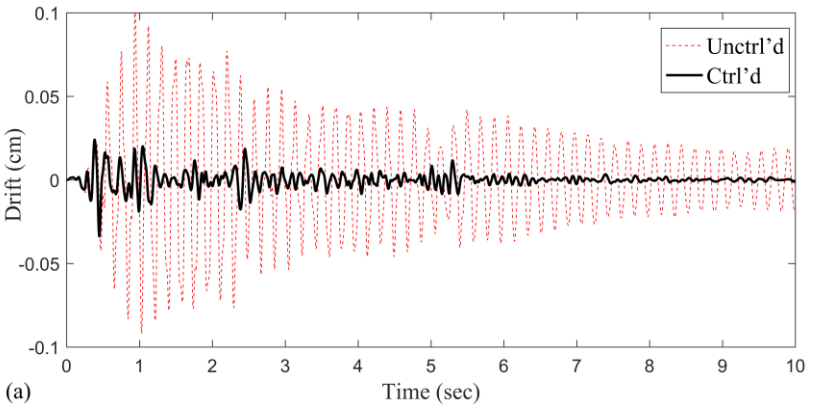

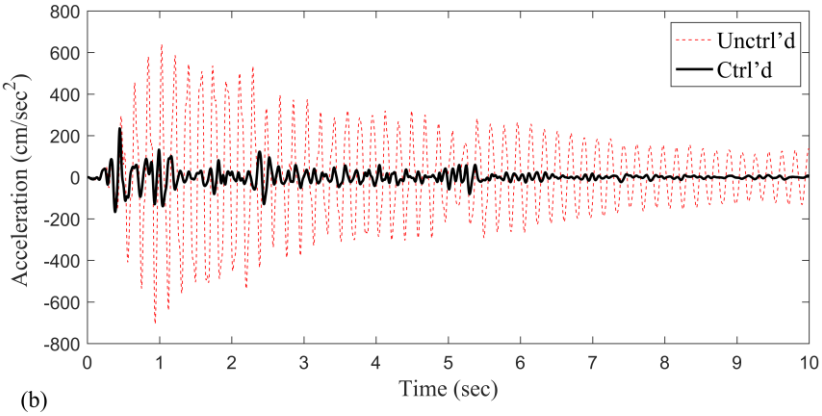

Figure 8. Time histories of responses on the third floor under the low (50%) El Centro earthquake: (a) drift; and (b) acceleration

Tables 3 to 5 reported the maximum drift and acceleration of the stories under the different levels of the El Centro earthquake for the uncontrolled, passive-off, passive-on, and

[DOI: 10.22068/ijoce.2024.14.4.608]

the SSC strategy. To evaluate the performance of the designed SSC in compared to the other well–known controllers, the results of the clipped-optimal [6] and the semi-active fuzzy control [9] strategies were shown in Tables 3 to 5. As can be seen from Tables 3 to 5, the results demonstrate that the SSC strategy provided the considerable reduction of the structural maximum drift and acceleration of the stories subjected to the different levels of the El Centro earthquake. The results in Tables 3 to 5 also show that using the SSC strategy the mean of the maximum drifts over the height of the building was respectively obtained by 0.066, 0.104, and 0.033 cm under the normal, high, and low levels. Using the fuzzy control [9], the mean of the maximum drifts was by 0.113, 0.159, and 0.058 cm under the normal, high, and low levels, respectively. In the term of the maximum accelerations, the mean values of 294.2, 457.4, and 166.3 cm/sec^2 were respectively reported for the SSC strategy under the normal, high, and low levels. For the fuzzy control [9], the mean values of 514.0, 661.3, and 245.0 cm/sec^2 were achieved under the normal, high, and low levels, respectively. Thus, the overall performance of the SSC strategy is much superior that of the fuzzy control [9] and clipped-optimal [6] strategies.

Table 3: Comparative performance of different control strategies in the normal level of the El Centro earthquake

Structural response	Parameter	Unctrl'd	P-Off	P-On	Clipped-optimal	Fuzzy	SSC
Maximum drift (cm)	d_1	0.549	0.211	0.079	0.114	0.101	0.091
	d_2	0.318	0.153	0.157	0.90	0.137	0.0617
	d_3	0.203	0.103	0.111	0.101	0.101	0.041
	Mean	0.357	0.156	0.116	0.37	0.113	0.066
Maximum acceleration (cm/s^2)	$\ddot{x}_1$	882	423	291.3	721	400	259.1
	$\ddot{x}_2$	1065	490.6	501.8	746	438	239.3
	$\ddot{x}_3$	1412	725.5	771.7	706	704	399.0
	Mean	1119.7	546.4	521.6	724.3	514	299.1

Table 4: Comparative performance of different control strategies in the high level of the El Centro earthquake

Structural response	Parameter	Unctrl'd	P-Off	P-On	Clipped-optimal	Fuzzy	SSC
Maximum drift (cm)	d_1	0.823	0.348	0.136	0.178	0.164	0.153
	d_2	0.477	0.251	0.219	0.126	0.185	0.099
	d_3	0.304	0.165	0.154	0.142	0.127	0.060
	Mean	0.535	0.255	0.170	0.149	0.159	0.104
Maximum acceleration (cm/s^2)	$\ddot{x}_1$	1323	616.94	510.07	959	547	370.53
	$\ddot{x}_2$	1598.2	757.1	623.30	1054	552	395.70
	$\ddot{x}_3$	2118.7	1153	1081.10	985	885	625.91
	Mean	1680	842.34	738.17	999.33	661.33	464.05

[DOI: 10.22068/ijoce.2024.14.4.608]

Table 5: Comparative performance of different control strategies in the low level of the El Centro earthquake

Structural response	Parameter	Unctrl'd	P-Off	P-On	Clipped-optimal	Fuzzy	SSC
Maximum drift (cm)	d_1	0.274	0.091	0.039	0.053	0.051	0.038
	d_2	0.159	0.066	0.079	0.053	0.072	0.038
	d_3	0.101	0.038	0.056	0.051	0.051	0.024
	Mean	0.178	0.065	0.058	0.052	0.058	0.033
Maximum acceleration (cm/s^2)	$\ddot{x}_1$	441.0	193.8	145.8	447	188	146.9
	$\ddot{x}_2$	532.7	219	252.4	354	192	143.5
	$\ddot{x}_3$	706.2	262.9	387.3	356	355	234.9
	Mean	560	225.3	261.8	385.7	245	175.1

In order to compare the seismic performance of the SSC strategy with the other control methods, the mean of the reduction percentages of the maximum drifts and accelerations for all stories was depicted in Figs. 9 to 11 for the normal, high, and low levels of the El Centro earthquake, respectively. The results show that for the normal, high, and low levels the mean of the reduction percentages of the maximum responses over the height of the building was respectively decreased by 81.4, 80.55, and 81.46% for the drifts and by 73.73, 72.37, and 68.7% for the accelerations. Further, the mean of the reduction percentages obtained the semi-active SSC system with the semi-active clipped-optimal and fuzzy systems is highest value under the different levels of the El Centro earthquake. It is demonstrated that the semi-active SSC system is very effective in reducing the structural responses due to the different levels of the El Centro earthquake.

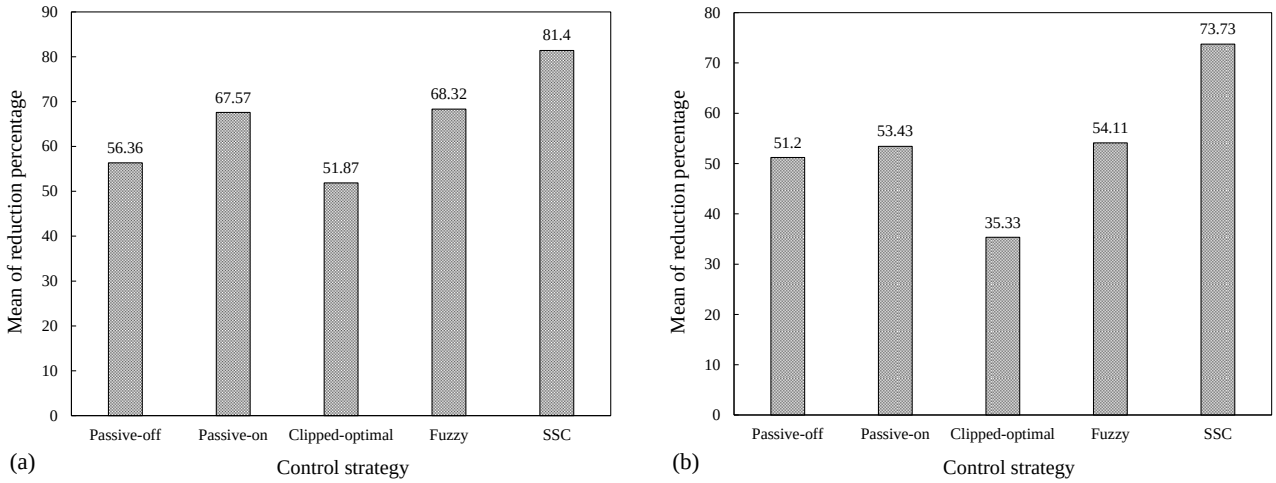

Figure 9. Mean of reduction percentage of responses on the third floor under the normal (100%) El Centro earthquake: (a) drift; and (b) acceleration

[DOI: 10.22068/ijoce.2024.14.4.608]

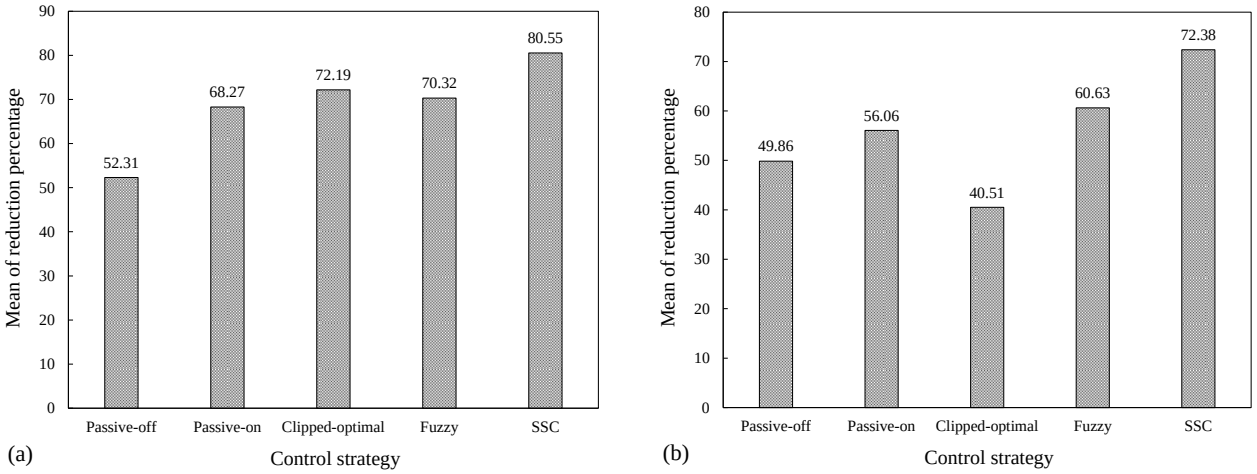

Figure 10. Mean of reduction percentage of responses on the third floor under the high (150%) El Centro earthquake: (a) drift; and (b) acceleration

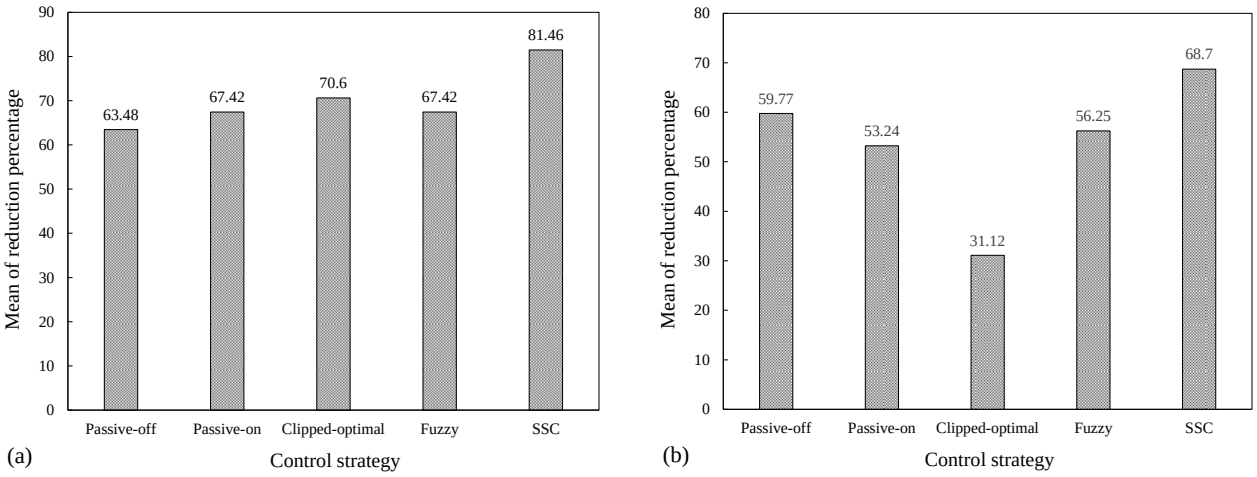

Figure 11. Mean of reduction percentage of responses on the third floor under the low (50%) El Centro earthquake: (a) drift; and (b) acceleration

In the all levels of the El Centro earthquake, the performance results of the semi-active SSC controller depicetd in Figs. 9 to 11 were better than those of the passive controllers of the MR damper. Finally, the maximum force in the MR damper generated in the different levels was reported in Table 6 in order to compare the performance of the different strategies in taking more benefits of the MR capacity. As can be seen from Table 6, the peak control force of the semi-active fuzzy SSC system is relatively small compared to that of the passive-on system, the semi-active clipped-optimal and fuzzy control systems.

[DOI: 10.22068/ijoce.2024.14.4.608]

Table 6: Comparison of control strategies performance for the control force during three levels of El Centro earthquake

Control strategies	Passive-off (N)	Passive-on (N)	Clipped-optimal (N)	Fuzzy (N)	SSC (N)
Standard-level	259.7	993.7	953	843	612.9
High-level	363.8	1187.5	1163	969	920.5
Low-level	160.7	492	421	393	354.7

7. CONCLUSIONS

A semi-active SSC strategy using a MR damper was presented for the seismic control of a 3–story building structure. The SSC strategy directly produced the desired command voltage. The effectiveness of the SSC strategy with the MR damper was demonstrated in reducing the structural responses for a wide range of loading conditions and was compared with the passive-off, passive-on conditions and the semi-active clipped-optimal and fuzzy strategies. The results show that the semi-active SSC strategy efficiently reduced the mean of the maximum responses over the height of the structure by 81.4, 80.55, and 81.46% for the drifts and by 73.73, 72.37, and 68.7% for the accelerations under the different levels of the El Centro earthquake. Further, it was indicated that the semi-active SSC system in comarison with the semi-active clipped-optimal and fuzzy strategies was very effective in reducing the structural responses due to the different levels of the El Centro earthquake. For the same capacity of the MR damper, the maximum control force produced by the SSC strategy was found to be little less in comparison with that of the clipped-optimal and fuzzy strategies. Finally, the better performance of the seismic control was achieved by the semi-active SSC strategy while requiring smaller control force was required in comparison with the passive-on controller.

REFERENCES

1. Kaveh A, Fahimi Farzam M, Jalali HH. Statistical seismic performance assessment of tuned mass damper inerter. *Struct Control Health Monit.* 2020;**27**(6).
2. Kaveh A, Mohammadi S, Khadem Hosseini O, Keyhani A, Kalatjari VR. Optimum parameters of tuned mass dampers for seismic applications using charged system search. *Iran J Sci Technol.* 2015;**39**(C1):21-40.
3. Hrovat D, Barak P, Rabins M. Semi-active versus passive or active tuned mass dampers for structural control. *J Eng Mech.* 1983;**109**(3):691–705.
4. Connor J, Laflamme S. *Structural Motion Engineering.* Springer; 2014.
5. Soong TT, Spencer BF. Active, semi-active and hybrid control of structures. *Bull New Zeal Soc Earthq Eng.* 2000;**33**(3):387–402.

[DOI: 10.22068/ijoce.2024.14.4.608]

6. Dyke SJ, Spencer BF Jr, Sain MK, Carlson JD. Modeling and control of magnetorheological dampers for seismic response reduction. *Smart Mater Struct.* 1996;**5**(5):565.
7. Spencer BF, Sain MK. Controlling buildings: a new frontier in feedback. *IEEE Control Syst Mag.* 1997;**17**(6):19–35.
8. Jansen LM, Dyke SJ. Semiactive control strategies for MR dampers: comparative study. *J Eng Mech.* 2000;**126**(8):795–803.
9. Choi K, Cho S, Jung H, Lee I. Semi-active fuzzy control for seismic response reduction using magnetorheological dampers. *Earthq Eng Struct Dyn.* 2004;**33**(6):723–36.
10. Qin X, Zhang X, Sheldon C. Study on semi-active control of mega-sub controlled structure by MR damper subject to random wind loads. *Earthq Eng Eng Vib.* 2008;**7**:285–94.
11. Rodríguez A, Pozo F, Bahar A, et al. Force-derivative feedback semi-active control of base-isolated buildings using large-scale MR fluid dampers. *Struct Control Health Monit.* 2012;**19**(1):120–45. doi:10.1002/stc.430.
12. Khalid M, Yusof R, Joshani M, Selamat H, Joshani M. Nonlinear identification of a magneto-rheological damper based on dynamic neural networks. *Comput Civ Infrastruct Eng.* 2014;**29**(3):221–33.
13. Mohebbi M, Bagherkhani A. Optimal design of magneto-rheological dampers. *Int J Optim Civ Eng.* 2014;**4**(3):361–80.
14. Kaveh A, Pirgholizadeh S, Khadem Hosseini O. Semi-active tuned mass damper performance with optimized fuzzy controller using CSS algorithm. *Asian J Civ Eng.* 2015;**16**(5):587-606.
15. Cha Y, Agrawal AK. Seismic retrofit of MRF buildings using decentralized semi-active control for multi-target performances. *Earthq Eng Struct Dyn.* 2017;**46**(3):409–24.
16. Zabihi-Samani M, Ghanooni-Bagha M. Optimal semi-active structural control with a wavelet-based cuckoo-search fuzzy logic controller. *Iran J Sci Technol Trans Civ Eng.* 2019;**43**(4):619–34.
17. Payandeh-Sani M, Ahmadi-Nedushan B. Semi-active neuro-control for minimizing seismic response of benchmark structures. *IUST.* 2022;**12**(1):47–67. Available at: http://ijoce.iust.ac.ir/article-1-504-en.html.
18. Bathaei A, Zahrai SM. Improving semi-active vibration control of an 11-story structure with non-linear behavior and floating fuzzy logic algorithm. *Structures.* 2022;132–146.
19. Bagherkhani A, Mohebbi M. Optimal design of MR dampers by considering design criteria and dampers distribution effect. *Iran J Sci Technol Trans Civ Eng.* 2022;**46**(6):4093–109.
20. Zizouni K, Saidi A, Fali L, Bousserhane IK, Djermane M. Semi-active structural vibrations control with magneto-rheological damper based on the hybrid fuzzy sliding mode controller. *Rev la construcción.* 2023;**22**(1):36–50.

[DOI: 10.22068/ijoce.2024.14.4.608]

21. Jalali HH, Farzam MF, Gavgani SAM, Bekdaş G. Semi-active control of buildings using different control algorithms considering SSI. *J Build Eng.* 2023;**67**:105956.
22. Payandeh-Sani M, Ahmadi-Nedushan B. Optimal placement of magneto-rheological dampers using nsga-ii-based fuzzy control. *IUST.* 2023;**13**(2):189–205. doi:10.22068/ijoce.2023.13.2.549.
23. Furuta K. Sliding mode control of a discrete system. *Syst Control Lett.* 1990;**14**(2):145–52.
24. Furuta K, Pan Y. Variable structure control with sliding sector. *Automatica.* 2000;**36**(2):211–28.
25. Iwase M, Furuta K. Sliding sector control using new equivalent sector control. *Int J Control.* 2020;**93**(2):238–51.
26. Ozcan S, Salamci MU, Nalbantoglu V. Nonlinear sliding sector design for multi-input systems with application to helicopter control. *Int J Robust Nonlinear Control.* 2020;**30**(6):2248–91.
27. Spencer BF, Dyke SJ, Sain MK, Carlson JD. Phenomenological model for magnetorheological dampers. *J Eng Mech.* 1997;**123**(3):230–38. doi:10.1061/(asce)0733-9399(1997)123:3(230).
28. Saadatfar S, Emami F, Khatibinia M, Eliasi H. Sliding sector–based adaptive controller for seismic control of structures equipped with active tuned mass damper. *Structures.* 2023;**51**:1507–24. doi:10.1016/j.istruc.2023.03.117.
29. Dyke BSJ, Spencer BF Jr, Quast P, et al. Acceleration feedback control of mdof structures. *ASCE.* 1996;907–918.
30. Eliasi H, Yazdani H, Khatibinia M, Mahmoudi M. Optimum design of a sliding mode control for seismic mitigation of structures equipped with active tuned mass dampers. *Struct Eng Mech.* 2022;**81**(5):633–45. doi:10.12989/sem.2022.81.5.633.
31. Khatibinia M, Mahmoudi M, Eliasi H. Optimal Sliding Mode Control for Seismic Control of Buildings Equipped With ATMD. *Iran Univ Sci Technol.* 2020;**10**(1):1–15. Available at: http://ijoce.iust.ac.ir/article-1-417-en.html.

[DOI: 10.22068/ijoce.2024.14.4.608]